# Vortex motion and nonlinear response in coupled noisy phase oscillator lattices under shear stress

Hidetsugu Sakaguchi

*Interdisciplinary Graduate School of Engineering Sciences, Kyushu University, Kasuga, Fukuoka 816-8580, Japan*

Vortex motion in coupled phase oscillator lattices is analogous to the dislocation motion in crystals. A single vortex exhibits a glide motion by force at the boundaries. Thermal fluctuations induce the glide motion even below the critical point corresponding to the Peierls stress. The random drift motion is approximated as a random walk in a tilted potential. If the temperature is high, vortices are spontaneously generated. A nonlinear response where the frequency profile is relatively flat in the central region and changes sharply near the boundaries is observed when the vortex density becomes large and nonuniform.

## I. INTRODUCTION AND MODEL EQUATION

Coupled phase oscillators have been intensively studied by many authors as a simple solvable model of coupled limit-cycle oscillators since the original Kuramoto model [1–5]. In the phase oscillator models, the limit-cycle oscillators are expressed with oscillation phase. The original Kuramoto model has a global coupling, and the mean-field approximation can be applied. Coupled phase oscillators on square or cubic lattices called oscillator lattices are also important, since locally coupled systems are more common [6,7]. For example, a sheet of beating heart cells is produced in bioengineering.

On the other hand, strongly deformed solids exhibit various nonlinear phenomena such as a fracture in brittle materials and plastic flow in ductile materials. Plasticity mechanics is one of the basic research fields of solid materials. In strongly deformed materials, many dislocations are spontaneously generated. The screw and edge dislocations are typical line defects in crystals. The dynamics of dislocations is a fundamental process in the mechanics of plasticity [8,9]. The mobility of dislocations in crystals and the nonlinear plastic flows in solids have been studied by many authors [10–12]; however, the understanding still needs to complete.

Suppose the phase in the oscillator lattice is interpreted as the one-dimensional displacement from the equilibrium position in crystals; the vortex in the phase oscillator lattice corresponds to the dislocation. The shear stress in the dislocation theory corresponds to the external force for phase oscillators on the boundaries. The average velocity of plastic flow corresponds to the average frequency of phase oscillators.

In a previous paper, we studied various deterministic dynamics of vortices and vortex lines in the phase oscillator lattices with inertia [13]. The model equation is expressed as

$$\frac{d^2\phi_{i,j}}{dt^2} = K \sum_{i',j'} \sin(\phi_{i',j'} - \phi_{i,j}) - d\frac{d\phi_{i,j}}{dt} + f_{i,j}, \quad (1)$$

where $(i', j')$'s are the four nearest-neighbor sites of the $(i, j)$ site on the rectangular lattice of $L_x \times L_y$, $K$ is the coupling constant, and $d$ is the parameter of viscosity. If $d = 0$, $f_{i,j} = 0$, and the phase difference $\phi_{i',j'} - \phi_{i,j}$ is sufficiently small, then the continuum approximation of Eq. (1) is expressed as

$$\frac{\partial^2\phi}{\partial t^2} = K\left(\frac{\partial^2\phi}{\partial x^2} + \frac{\partial^2\phi}{\partial y^2}\right). \quad (2)$$

This equation is the equation of motion of the two-dimensional elastic body if $\phi$ is assumed to be the displacement in the $z$ direction. The parameter $K$ corresponds to $\mu/\rho$, where $\mu$ is the modulus of rigidity and $\rho$ is the density of the elastic body. As a model of the shear stress, the external force $f_{i,j}$ is applied at the boundaries in the $y$ direction as $f_{i,j} = F$ at $j = L_y$ and $f_{i,j} = -F$ at $j = 1$. The external force $f_{i,j}$ is zero for the other lattice points.

We found that the vortex begins to move if the shear stress is beyond a critical force, which corresponds to the Peierls stress in the dislocation theory. We numerically found that the vortex exhibits a stick-slip motion when the viscous friction coefficient $d$ is sufficiently small. The pair annihilation of vortex and antivortex occurs for large $d$; however, the vortices pass through each other when $d$ is small. New vortices are created when $F$ is large, and chaotic behavior appears. The time-average frequency jumps at the phase slip region where the vortices move almost in the $x$ direction. This corresponds to the plastic flow via the dislocation motion in the theory of plasticity.

In this paper, we will study a coupled noisy phase oscillator lattice under the shear-stress-type force. The external force is applied at the boundaries in the $y$ direction, and the boundaries play the role of pacemaker for the coupled phase oscillators. A two-dimensional coupled noisy phase oscillator lattice is obtained by removing the inertia term $d^2\phi_{i,j}/dt^2$ at $d = 1$ and adding the noise term to Eq. (1):

$$\frac{d\phi_{i,j}}{dt} = K \sum_{i',j'} \sin(\phi_{i',j'} - \phi_{i,j}) + f_{i,j} + \xi_{i,j}(t), \quad (3)$$

where the Gaussian white noises satisfy $\langle \xi_{i,j}(t)\xi_{i',j'}(t')\rangle = 2T\delta_{i,i'}\delta_{j,j'}\delta(t-t')$. If $f_{i,j}$ takes a random number, then the synchronization cluster expands with the increase of $K$ in Eq. (3) at $T = 0$; however, there is no Kuramoto-type phase transition in two dimensions as we studied in Ref. [6]. If the spatial dimension is higher, then the random oscillator lattices can exhibit a transition similar to the Kuramoto-type phase transition, as discussed in Refs. [6] and [7]. In this paper, the external force is set to be $f_{i,j} = F$ at $j = L_y$, $f_{i,j} = -F$ at $j = 1$, and $f_{i,j} = 0$ for the other sites, which is interpreted as the shear stress in this paper.

If $f_{i,j} = 0$, then the stationary state of the Langevin equation (3) is a thermal equilibrium state. The probability distribution of $\phi_{i,j}$ is expressed as

$$P(\{\phi_{i,j}\}) \propto \exp\left\{-K\sum\cos(\phi_{i',j'}-\phi_{i,j})/(2T)\right\}.$$

This equilibrium distribution is equivalent to that of the two-dimensional $XY$ spin system. The Kosterlitz-Thouless transition occurs at $T_K = (\pi/4)K$ [14]. For $T > T_K$, many free vortices are generated by thermal fluctuations, and the spatial correlation decays exponentially in contrast to the power-law decay for $T < T_K$. The external force $F$ induces a nonequilibrium state. The external force might not be easily applied in the $XY$ spin system; however, a similar nonequilibrium state might be realized by using counter-rotating magnetic fields at the boundaries $j = 1$ and $L_y$ in the $XY$ spin systems.

In a solid, $F$ corresponds to the shear stress, and the vortex corresponds to the screw dislocation. The shear stress generates the Peach-Koehler force, which induces the glide motion of the dislocation in the $x$ direction if the shear stress is beyond the Peierls stress [8,9]. We confirmed the glide motion using Eq. (1) in the previous paper. The vortex can move due to thermal fluctuations even if the shear stress is below the Peierls stress. The density and the motion of dislocations are critical to determining the mechanical property of solids and the electrical property of semiconductor devices. The dislocation motion at a finite temperature has been experimentally studied by many authors [15]. The dislocation velocity is often approximated by $v \propto \tau^m \exp(-\Delta E/T)$, where $\tau$ is the shear stress, $m$ is a fitting parameter of the power law, and $T$ is the temperature, although the physical origin is not clear. We will study the motion of a single vortex in the coupled noisy phase oscillator lattice under the shear stress in Sec. III. We try to approximate the vortex motion as the Brownian motion in a tilted periodic potential explained in Sec. II.

When the noise strength is larger, many vortices are spontaneously generated. We will study the average frequency profile in Sec. IV. The frequency profile is not a linear function of $j$, i.e., relatively flat in the central region and changes sharply near the boundaries where the shear stress is applied. Our model can be considered a typical problem of nonequilibrium statistical mechanics.

## II. BROWNIAN MOTION IN A TILTED POTENTIAL

In this section, we explain the Brownian motion under the external force, which has been studied as a typical nonequilibrium phenomenon, for the application to the vortex motion in the subsequent section. An overdamped one-dimensional

Brownian motion in a tilted sinusoidal potential is described with the Langevin equation:

$$\eta\frac{dx}{dt} = -a\sin(2\pi x) + f + \xi(t),\tag{4}$$

where $\eta$ denotes the viscous friction coefficient, $a$ is the amplitude of the periodic potential with spatial period 1, and $f$ is the external force. The Gaussian noise $\xi(t)$ is assumed to satisfy $\langle \xi(t)\xi(t')\rangle = 2D\delta(t-t')$. Here $D$ satisfies $D = \eta T$ where $T$ is temperature owing to the fluctuation-dissipation theorem. The average velocity of $x$ is expressed as [16]

$$\left\langle\frac{dx}{dt}\right\rangle = \frac{1-e^{-f/T}}{\int_{-1/2}^{1/2} I_+(x)dx},\tag{5}$$

where

$$I_+(x) = \frac{\eta}{T}\int_0^1 e^{\{V_0(x)-V_0(x-y)-yf\}/T}dy.\tag{6}$$

Here the potential $V_0(x)$ is expressed as $V_0(x) = -a\cos(2\pi x)/(2\pi)$.

Next, we consider a simple system of linearly coupled two Brownian particles [17] to understand the Brownian motion of the center of mass. The model equations are assumed to be

$$\frac{dx_1}{dt} = -b\sin(2\pi x_1) + f + k(x_2 - x_1) + \xi_1(t),$$

$$\frac{dx_2}{dt} = -b\sin(2\pi x_2) + f + k(x_1 - x_2) + \xi_2(t),\tag{7}$$

where the Gaussian noises satisfy $\langle \xi_i(t)\xi_j(t')\rangle = 2D_0\delta_{i,j}\delta(t-t')$ and the viscous friction coefficient $\eta$ is set to 1. The mass center $y = (x_1 + x_2)/2$ and the relative coordinate $z = (x_2 - x_1)/2$ obey

$$\frac{dy}{dt} = -b\cos(2\pi z)\sin(2\pi y) + f + \xi_1'(t),\tag{8}$$

$$\frac{dz}{dt} = -b\cos(2\pi y)\sin(2\pi z) - 2kz + \xi_2'(t),\tag{9}$$

where the Gaussian noises satisfy $\langle \xi_i'(t)\xi_j'(t')\rangle = D_0\delta_{i,j}\delta(t-t')$. The mass center $y$ obeys the Langevin equation similar to Eq. (4). The viscous friction coefficient for the mass center $y$ is 1, the amplitude of the sinusoidal potential changes in time as $b\cos(2\pi z(t))$, and the effective temperature decreases to $D = D_0/2$. The corresponding Fokker-Planck equation for the probability density $P(y,z)$ is described as

$$\frac{\partial P}{\partial t} = -\frac{\partial}{\partial y}\left(-\frac{\partial V}{\partial y}P\right) - \frac{\partial}{\partial z}\left(-\frac{\partial V}{\partial z}P\right) + D\left(\frac{\partial^2 P}{\partial y^2} + \frac{\partial^2 P}{\partial z^2}\right),\tag{10}$$

where the potential $V$ is given by

$$V(y,z) = \left[-\frac{b}{2\pi}\cos(2\pi y)\cos(2\pi z) - fy + kz^2\right].\tag{11}$$

The periodic boundary condition $P(y,z) = P(y+1,z)$ is assumed.

We have performed direct numerical simulations of the coupled Langevin equations Eqs. (8) and (9) and the Fokker-Planck equation Eq. (10) for $b = 1$, $D_0 = 0.2$, and $k = 2.5$. Figure 1 shows the average velocities (rhombi) for several $f$'s
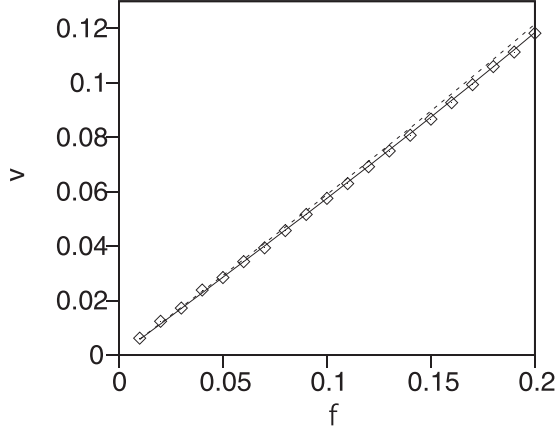
FIG. 1. Comparison of the average velocities by the coupled Langevin equations (rhombi), the Fokker-Planck equation (solid line) at $f = 0.01n$ ($n = 1, 2, \ldots, 20$) for $b = 1$, $D_0 = 0.2$, and $k = 2.5$. The dashed line is Eq. (5) at $a = 0.674$, $\eta = 1$, and $T = D = D_0/2 = 0.1$.

obtained by the coupled Langevin equations and $\langle -\partial V/\partial y \rangle$ (solid line) obtained by the direct numerical simulation of the Fokker-Planck equation. The two kinds of velocities take almost the same values. The average value of $\cos(2\pi z)$ for $b = 0$ in Eq. (9) is given by

$$\langle \cos(2\pi z) \rangle = e^{-D\pi^2/k} \simeq 0.674.$$

Equation(8) can be approximated at Eq. (4) with $a = e^{-D\pi^2/k}b$ and $D = 0.1$. The dashed line in Fig. 1 denotes the average velocity given by Eq. (5) at $a = 0.674$ and $D = 0.1$. Figure 1 shows that the approximation by the one-dimensional Langevin equation Eq. (4) with modified parameters $D = D_0/2$ and $a = e^{-D\pi^2/k}b$ is fairly good. This example demonstrates the usefulness of modeling by the one-dimensional Langevin equation Eq. (4) for the stochastic dynamics of the mass center.

## III. MOTION OF A SINGLE VORTEX IN NOISY PHASE OSCILLATOR LATTICES

In this section, we study a vortex motion in the coupled noisy phase oscillators on the square lattice:

$$\frac{d\phi_{i,j}}{dt} = K \sum_{i',j'} \sin(\phi_{i',j'} - \phi_{i,j}) + f_{i,j} + \xi_{i,j}(t).$$

No-flux boundary conditions are imposed at $i = 1$, $i = L_x$, $j = 1$, and $j = L_y$. Initially, a vortex is set at the center by assuming the phase profile to be

$$\phi_{i,j} = \phi_{i,j}^0 = \cos^{-1}(x/r). \text{ for } y > 0, \text{ and}$$

$$\phi_{i,j} = \phi_{i,j}^0 = 2\pi - \cos^{-1}(x/r). \text{ for } y < 0, \quad (12)$$

where $x = i - (L_x + 1)/2$, $y = j - (L_y + 1)/2$, and $r = \sqrt{x^2 + y^2}$. There is a phase singularity or a vortex at $x = y = 0$. The external force $f_{i,j}$ is applied only at the boundaries in the $y$ direction, that is, $f_{i,j} = F$ at $j = L_y$ and $f_{i,j} = -F$ at $j = 1$. The external force is set to zero for the other lattice
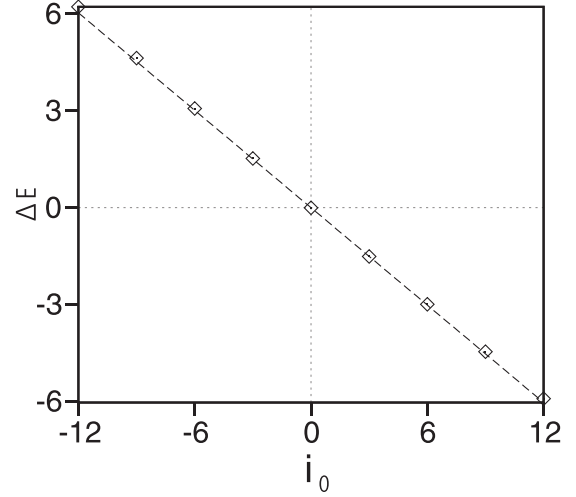


FIG. 2. Energy difference $\Delta E$ as a function of the vortex center $i_0$ from the energy at $i_0 = 0$ for $F = 0.08$.

points. The Gaussian white noise $\xi_{i,j}$ is applied for $1 < j < L_y$.

First, we have performed numerical simulation with the Runge-Kutta method with timestep $\Delta t = 0.005$ in case of $T = 0$. The system size is $1000 \times 100$. The vortex does not move for $F < F_c = 0.100165$. The vortex is trapped by the periodic potential of the oscillator lattice. The effective potential corresponds to the Peierls potential in the dislocation theory. We have calculated the total energy:

$$E = -\frac{K}{2} \sum_{i',j',i,j} \cos(\phi_{i',j'} - \phi_{i,j}) - F \sum_i \phi_{i,L_y} + F \sum_i \phi_{i,1} \quad (13)$$

for the stationary state obtained from the initial conditions $\phi_{i,j} = \phi_{i-i_0,j}^0$, where the vortex center is shifted by $i_0$ in the $x$ direction. Figure 2 shows the difference $\Delta E = E(i_0) - E(i_0 = 0)$ for $F = 0.08 < F_c$. The dashed line is $\Delta E = -2\pi F i_0$. The energy linearly decreases in proportion to $2\pi F$. Here $2\pi$ corresponds to the magnitude of the Burgers vector, $F$ to the shear stress, and $2\pi F$ to the Peach-Koehler force in the dislocation theory. The Peach-Koehler force $2\pi F$ drives the glide motion of the vortex.

If $F > F_c$, then the vortex moves in the $x$ direction. Figure 3(a) shows the average velocity of the vortex as a function of $F$. This motion is similar to the particle motion in a tilted spatially periodic potential expressed by Eq. (4) at $D = 0$. The average velocity of the particle for Eq. (4) at $D = 0$ is given by

$$v = \frac{\sqrt{F^2 - F_c^2}}{\eta},$$

for $F > F_c = a$. Figure 3(b) shows the relationship between $F - F_c$ and $\eta = \sqrt{F^2 - F_c^2}/v$ using the velocities $v$'s obtained by the direct numerical simulation. The effective viscous friction coefficient decreases with $F - F_c$. Figure 3(c) shows a relationship between the average velocity $v$ and the effective viscous friction $\eta$ in a semilogarithmic scale. A logarithmic divergence is observed at $F = F_c$. The dislocation motions in cellular structures for continuous dissipative
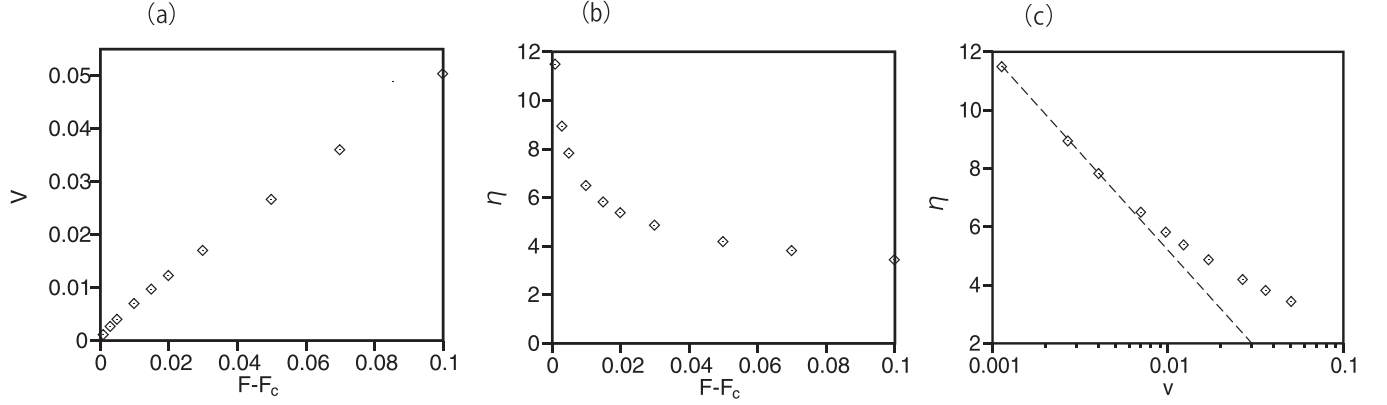
FIG. 3. (a) Velocity of the vortex when $F - F_c$ is changed. $F_c$ is 0.100165. (b) Effective friction coefficient $\eta$ as a function of $F - F_c$. (c) Relationship between the average velocity $v$ and the effective viscous friction $\eta$ in a semilogarithmic scale.

systems were studied by several authors [18]. The friction tensor corresponding to $\eta$ is expressed as [19]

$$D_{xx} = D_{yy} = \int \frac{\partial \psi}{\partial x} \frac{\partial \psi}{\partial x} dx dy = \int_{r_1}^{r_2} \int_0^{2\pi} \frac{\sin^2 \theta}{r^2} r dr d\theta$$

$$= \pi \ln(r_2/r_1), \quad D_{xy} = D_{yx} = 0, \quad (14)$$

where $\psi$ expresses the phase of the stationary solution including a dislocation and $r_2$ ($r_1$) is the upper (lower) limit of the integral. The logarithmic divergence in Fig. 3(c) is related to the logarithmic divergence of $D_{xx} = D_{yy} = \pi \ln(r_2)$ for our vortex solution in a discrete lattice with large $r_2$, Here the lower limit $r_1$ is set to be 1 of the lattice constant. If the vortex moves with velocity $v$, then the diffusion length of the diffusion type equation: $\partial \phi / \partial t = -v \partial \phi / \partial x = \partial^2 \phi / \partial x^2$ is estimated as $r_D = 1/v$. If $r_2$ is replaced with the diffusion length $r_D$, then $\eta \sim \log v$ is obtained, although this is a rough estimate.

Next, we have performed numerical simulation with the Heun method with timestep $\Delta t = 0.005$ in the case of $T \neq 0$ for $F < F_c = 0.100165$. The system size is assumed to be $500 \times 100$. Figure 4(a) shows the time evolution of the $X$ (solid line) and $Y$ (dashed line) coordinates of the vortex center at $T = 0.02\pi$ and $F = 0.08$. On average, the vortex

moves in the $x$ direction even for $F < F_c$ owing to the thermal fluctuations. The vortex exhibits a random motion around the average movement in the $x$ and $y$ directions. The rhombi in Fig. 4(b) shows the average velocities in the $x$ direction for several values of $T' \equiv T/(\pi/4)$ where $\pi/4$ is the critical temperature of the Kosterlitz-Thouless transition of the two-dimensional $XY$ model for $K = 1$. Here $F$ is set to be $F = 0.08$. The rhombi in Fig. 4(c) show the average velocities in the $x$ direction for several values of $F$ at $T' = 0.05$.

If the motion of the vortex core is approximated by Eq. (4), then the external force $f$ corresponds to $2\pi F$ and $a = 2\pi F_c$. The effective viscous friction $\eta$ and $D$ are unknown, but we can evaluate the values by fitting numerically obtained values to Eq. (5). The + marks in Fig. 4(b) show the velocities at $\eta = 20.66$ and $D = 22.3T'$ for $f = 2\pi F$ and $a = 2\pi F_c$. The effective temperature for the Brownian motion of the vortex center is valuated as $D/\eta = (22.3/20.66) \cdot T/(\pi/4) \simeq 1.37T$ using the fluctuation-dissipation relation. The effective temperature is slightly deviated from the temperature $T$ for each phase oscillator but takes a value close to $T$. Similarly, + marks in Fig. 4(c) shows the velocities at $\eta = 22.04$ and $D = 26.9T'$ for $f = 2\pi F$ and $a = 2\pi F_c$. These numerical results suggest that the approximation (+) by Eq. (4) is fairly good.
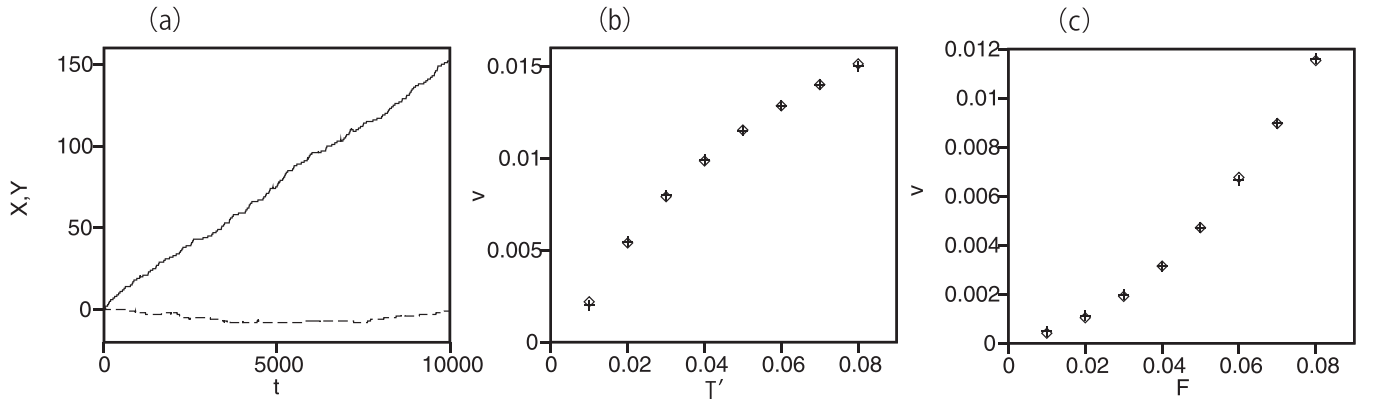


FIG. 4. (a) Time evolutions of $X$ (solid line) and $Y$ (dashed line) coordinates of the vortex center at $T = 0.02\pi$ and $F = 0.08$. (b) Average velocities (rhombi) in the $x$ direction for several values of $T'$ at $F = 0.08$. The + marks denote the velocities by Eq. (5) at $\eta = 20.66$ and $D = 22.3T'$. (c) Average velocities (rhombi) in the $x$ direction for several values of $F$ at $T' = 0.05$. The + marks denote the velocities by Eq. (5) at $\eta = 22.04$ and $D = 26.9T'$.
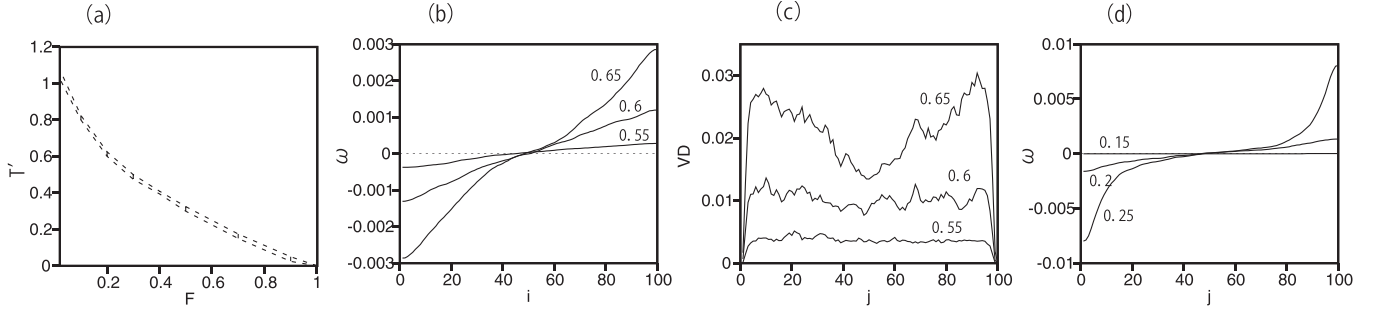
FIG. 5. (a) A guideline for the transition above which vortices are spontaneously generated. (b) Average frequency profile $\bar{\omega}_j$ at $T' = 0.55$, 0.6, and 0.65 for $F = 0.3$ and $L_y = 100$. (c) Number density of vortices at $T' = 0.55$, 0.6, and 0.65 for $F = 0.3$. (d) Average frequency profile $\bar{\omega}_j$ at $T' = 0.15$, 0.2, and 0.25 for $F = 0.7$.

## IV. FREQUENCY PROFILES IN NOISY PHASE OSCILLATOR LATTICES UNDER THE SHEAR FORCE

Figure 4 was the numerical results for relatively small $T'$. The vortex number is one during a finite time of the numerical simulation. However, thermal fluctuation generates vortex pairs spontaneously for higher temperature. We have performed numerical simulations in a system of $L_x \times L_y = 100 \times 100$ starting from the initial condition

$$\phi_{i,j} = \sin^{-1}(F/K)\{j - (L_y + 1)/2\}.$$

This phase configuration is a stable stationary solution in the case of $T = 0$, which represents a synchronized state for $F < K$ in a system with inhomogeneous natural frequencies: $f_{i,j} = -F$ at $j = 1$, $f_{i,j} = 0$ for $1 < j < L_y$, and $f_{i,j} = F$ at $j = L_y$. The no-flux boundary conditions are imposed at $j = 1$ and $j = L_y$, and the periodic boundary conditions are set at $i = 1$ and $i = L_x$. The completely synchronized state does not exist for $F > K$, and a desynchronization occurs at the critical value $F = K$ for the deterministic system of $T = 0$.

Figure 5(a) shows a transition line above which vortices are spontaneously generated. The transition line is only a guide, since there is no definite transition line in a stochastic system. We have performed numerical simulation until $t = t_f = 5 \times 10^5$ and calculated the frequency $\omega_{i,j} = \{\phi_{i,j}(t_f) - \phi_{i,j}(t_f/2)\}/(t_f/2)$ for each lattice point $(i, j)$. Figure 5(b) shows an average frequency profile $\bar{\omega}_j = \sum_{i=1}^{L_x} \omega_{i,j}/L_x$ at $T' = 0.55$, 0.6, and 0.65 for $F = 0.3$. The frequency profile is approximately a linear function of $j$ at $T' = 0.55$ and 0.6. The behavior is analogous to the Newtonian fluid. As $T'$ is larger, the slope of the frequency profile becomes larger. Besides, the frequency profile is not a linear function of $j$ at $T' = 0.65$. The slope of the frequency profile increases with the distance from the center $j = (L_y + 1)/2$ except for $j \simeq 1$ and $j \simeq L_y$. Figure 5(c) is the number density of vortices at $T' = 0.55$, 0.6, and 0.65 for $F = 0.3$. The vortex number increases with $T'$. The vortex number density fluctuates but is rather flat at $T' = 0.55$. However, the vortex density takes the maximum near the boundaries $j = 1$ and $L_y$ at $T' = 0.65$. The vortex number density is closely related to the nonlinearity of the frequency profile shown in Fig. 5(b). When the number density is flat, the frequency profile is almost a linear function of $j$. The inhomogeneous vortex density induces the nonlinear frequency profile. Figure 5(d) shows the average frequency profile at $T' = 0.15$, 0.2, and 0.25 for $F = 0.7$. The nonlinear-

ity appears slightly above the transition line shown in Fig. 5(a) at the larger value of $F$.

The average frequency profile $\bar{\omega}_j = \sum_{i=1}^{L_x} \omega_{i,j}/L_x$ is approximated at a cubic function $ay + by^3$, where $y = j - (L_y + 1)/2$. The parameters $a$ and $b$ are estimated from the numerically obtained data $\bar{\omega}_j$. Figure 6(a) compares numerically obtained frequency difference $\Delta\bar{\omega} = (\bar{\omega}_{97} - \bar{\omega}_4)/2$ with $ay + by^3$ at $y = 46.5$ for several values of $T'$ at $F = 0.5$. The approximation by the cubic function is rather good for the parameter range $0.2 < T' < 0.5$. Figure 6(b) shows $a$ and $b \times 10^3$ as a function of $T'$ for $F = 0.5$. The linear coefficient $a$ increases rapidly from $T' = 0.325$ and the nonlinear coefficient $b$ increases from $T' = 0.375$. That is, the shear flow owing to the vortex generation develops from $T' = 0.325$, and the nonlinearity shows up from $T' = 0.375$ for $F = 0.5$.

The nonlinear profile of the average frequency is observed even for different boundary conditions. As an example, we consider fixed boundary conditions of phase velocity. That is, the phase $\phi_{i,j}$ is assumed to be $\phi_{i,j} = \omega_0 t$ at $j = L_y$ and $\phi_{i,j} = -\omega_0 t$ at $j = 1$ like the Couette flow in fluid mechanics. Figure 7(a) shows the average frequency profiles at $\omega_0 = 0.0005$, 0.002, and 0.004 for $T' = 0.4$. For $\omega_0 < 0.0005$, the frequency profile is almost linear. However, the nonlinear frequency profiles become obvious for $\omega_0 \geqslant 0.002$, where the frequency profile changes rapidly near the two boundaries. Figure 7(b) shows the number density of vortices at $\omega_0 = 0.0005$ (dashed line) and 0.004 (solid line). The vortex density is roughly homogeneous at $\omega_0 = 0.0005$. However,
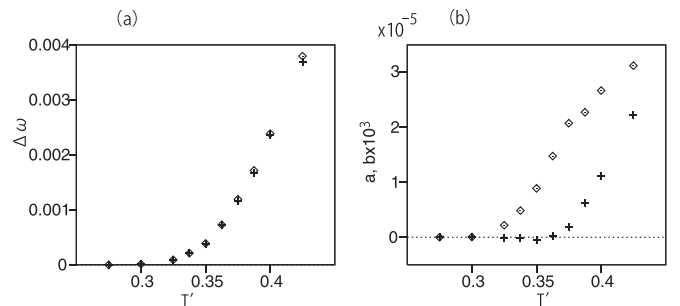


FIG. 6. (a) Numerically obtained frequency difference $\Delta\bar{\omega} = (\bar{\omega}_{97} - \bar{\omega}_4)/2$ and $ay + by^3$ for $y = 46.5$ for several $T'$ at $F = 0.5$. (b) The fitting parameters $a$ (rhombi) and $b \times 10^3$ (+) as a function of $T'$ at $F = 0.5$.
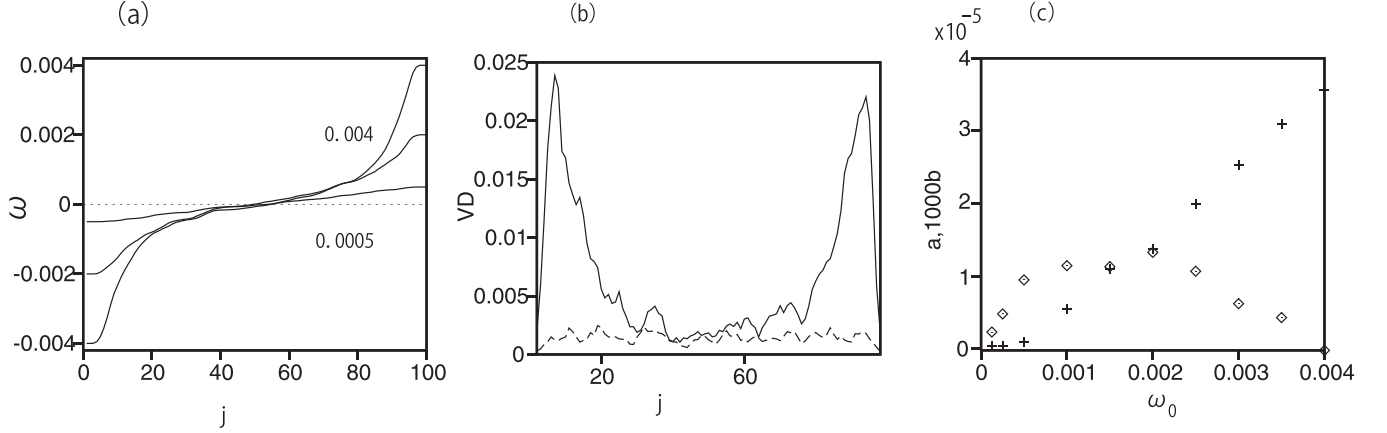
FIG. 7. (a) Average frequency profiles at $\omega_0 = 0.0005$, 0.002, and 0.004 for $T' = 0.4$. (b) Number density of vortices at $\omega_0 = 0.0005$ (dashed line) and 0.004 (solid line). (c) The fitting parameters $a$ (rhombi) and $b \times 10^3$ (+) as a function of $\omega_0$ at $T' = 0.4$.

there are two peaks of the vortex density near the boundaries at $\omega_0 = 0.004$. The nonlinear frequency profile is closely related to the inhomogeneous number density of vortices. Figure 7(c) shows the parameters $a$ and $b$ of the fitting curve $ay + by^3$, where $y = j - (L_y + 1)/2$ as a function of $\omega_0$. When $\omega_0$ is small, the parameter $b$ is nearly 0, and the linear fitting is a good approximation. The parameter $b$ increases with $\omega_0$ and $a$ decreases for $\omega_0 > 0.0025$. That is, the nonlinear response of the frequency profile appears even for these fixed boundary conditions of phase velocity.

We have studied the nonlinear response in larger systems. The system size is assumed to be $L_x \times L_y = 100 \times L_y$. The external force corresponding to the shear stress is fixed as $f_{i,L_y} = F$ and $f_{i,1} = -F$. We have calculated the frequency profiles and vortex density for $L_y = 200$, 400, and 600. Figure 8(a) shows the frequency profiles at $L_y = 200$, 400, and 600 at $T' = 0.65$ and $F = 0.3$. Notably, the frequency profiles overlap fairly well near the boundaries. The frequency slope increases with the distance from $j = (L_y + 1)/2$. The frequency profile tends to be flat near the center $j = L_y/2$ as $L_y$ is larger. We do not understand the frequency profile theoretically; however, the nonlinear response might be related to the so-called boundary layer in fluid mechanics [20]. It is known that many vortices are generated in the turbulent

boundary layer [21]. Our numerical result might also be related to the plug flow in the Bingham plastic fluid [22] and the shear banding [23,24] in some complex fluids, in which the velocity profile is not a linear function of $j$ but the slope of the velocity profile changes sharply at some points. Figure 8(b) shows the vortex density at $L_y = 600$ (solid line), 400 (dashed line), and 200 (dotted line) at $T' = 0.65$ and $F = 0.3$. The profiles of the vortex density also overlap fairly well near the boundaries. The vortex density is rather flat for large $L_y$ near $j = (L_y + 1)/2$. Figure 8(c) shows a relationship between $T'$ and the frequency at the boundary: $(\bar{\omega}_{L_y} - \bar{\omega}_1)/2$. Figure 8(c) shows that the shear flow appears for $T' \geqslant 0.55$ at $F = 0.3$.

We have furthermore studied the frequency profile and vortex number density in three-dimensional coupled noisy phase oscillator lattices. The model equation is expressed as

$$\frac{d\phi_{i,j,k}}{dt} = K \sum_{i',j',k'} \sin(\phi_{i',j',k'} - \phi_{i,j,k}) + f_{i,j,k} + \xi_{i,j,k}(t),$$

(15)

where $\xi_{i,j,k}(t)$ is the Gaussian white noise satisfying $\langle \xi_{i,j,k}(t)\xi_{i',j',k'}(t') \rangle = 2T\delta_{i,i'}\delta_{j,j'}\delta_{k,k'}\delta(t - t')$. The external force satisfies $f_{i,j,k} = 0$ for $2 \leqslant j \leqslant L_y$, $f_{i,j,k} = -F$ for $j = 1$, and $f_{i,j,k} = F$ for $j = L_y$. The system size is
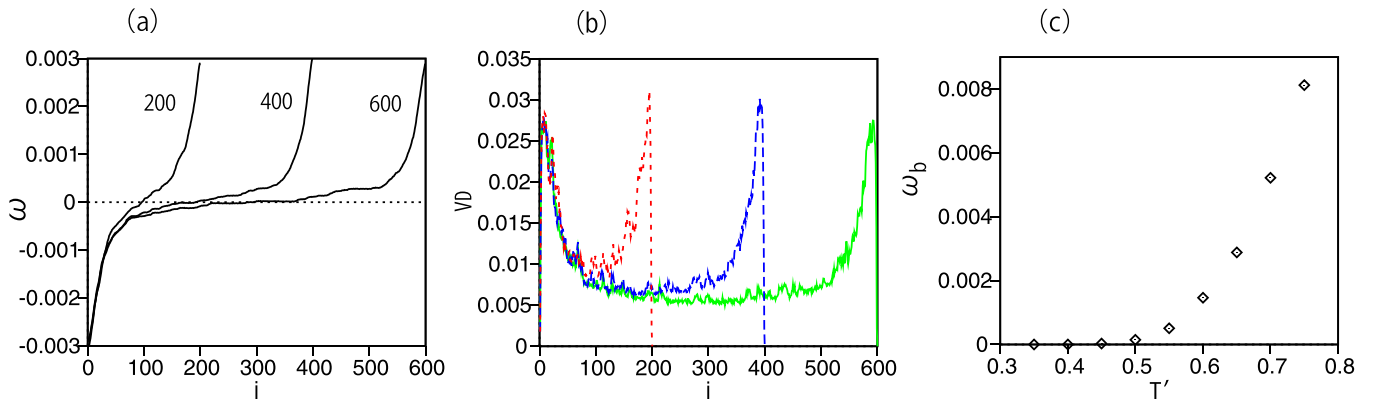


FIG. 8. (a) Average frequency profile $\bar{\omega}_j$ at $L_y = 200$, 400, and 600 at $T' = 0.65$ and $F = 0.3$. (b) Vortex density at $L_y = 600$ (solid green line), 400 (dashed blue line), and 200 (dotted red line) at $T' = 0.65$ and $F = 0.3$. (c) Frequency at the boundary as a function of $T'$.
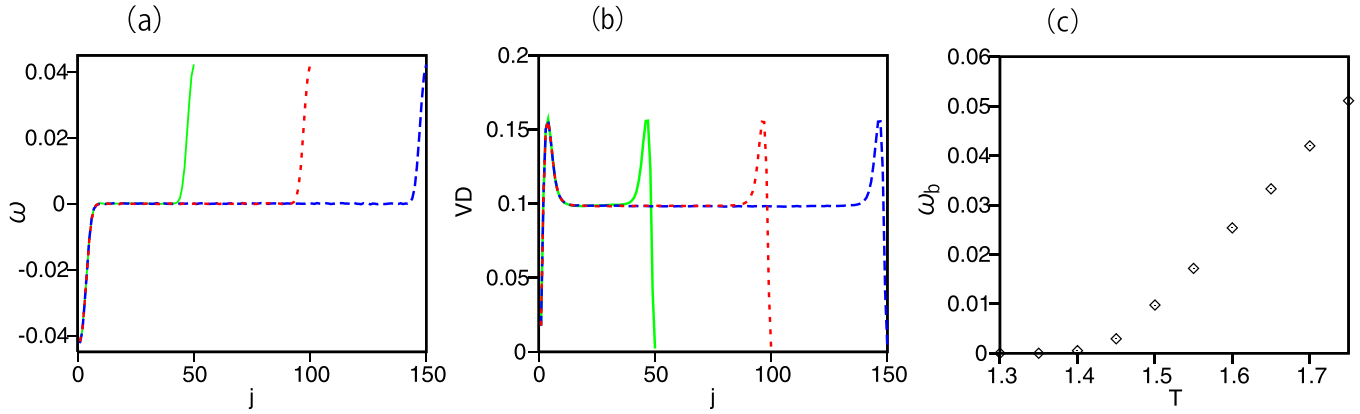
FIG. 9. (a) Average frequency profile $\bar{\omega}_j$ at $L_y = 50$ (solid green line), 100 (dotted red line), and 150 (dashed blue line) at $T = 1.7$ and $F = 0.3$. (b) Vortex density at $L_y = 50$ (solid green line), 100 (dotted red line), and 150 (dashed blue line) at $T = 1.7$ and $F = 0.3$. (c) Frequency $\omega_b$ at the boundary as a function of $T$.

$60 \times L_y \times 60$. Figure 9(a) shows the frequency profiles for $L_y = 50$, 100, and 150 at $T = 1.7$, $K = 1$, and $F = 0.3$. The frequency profiles overlap with each other near the boundaries. The average frequency becomes almost zero near the center $j \simeq L_y/2$. Figure 9(b) shows the vortex number density for $L_y = 50$, 100, and 150 at the same parameter values. The vortex number was calculated by the summation of absolute vorticity along all the elemental square loops such as $(i, j, k) \rightarrow (i + 1, j, k) \rightarrow (i + 1, j + 1, k) \rightarrow (i, j + 1, k) \rightarrow (i, j, k)$. The vortex number density also overlaps with each other near the boundaries. The number density takes a constant value near the center and increases near the boundaries. Figure 9(c) shows the relationship between $T$ and the frequency $\omega_b = (\omega_{L_y} - \omega_1)/2$. The nonzero frequency profile appears around $T \simeq 1.4$ for $F = 0.3$.

We have confirmed similar behaviors even in one-dimensional coupled noisy phase oscillator lattices. We have performed a numerical simulation of the model equation:

$$\frac{d\phi_j}{dt} = K \sum_{j'=j\pm1} \sin(\phi_{j'} - \phi_j) + \xi_j(t), \qquad (16)$$

where $\xi_j(t)$ is the Gaussian white noise satisfying $\langle \xi_j(t)\xi_{j'}(t') \rangle = 2T\delta_{j,j'}\delta(t - t')$. The system size is $L_y$. We show numerical results for the fixed-frequency boundary conditions: $\phi_1 = -Ft$ and $\phi_{L_y} = Ft$, although similar

numerical results were obtained in case that the external forces $\pm F$ are applied at $j = 1$ and $L_y$. The corresponding Fokker-Planck equation is written as

$$\frac{\partial P}{\partial t} = -\sum_{j=2}^{L_y-1} \frac{\partial}{\partial \phi_j}\left(-\frac{\partial V}{\partial \phi_j}P\right) + T\sum_{j=2}^{L_y-1}\frac{\partial^2 P}{\partial \phi_j^2}. \qquad (17)$$

The potential $V$ is given by

$$V = -\sum_{j=1}^{L_y-1} K\cos(\phi_j - \phi_{j+1}), \qquad (18)$$

where $\phi_1 = -Ft$ and $\phi_{L_y} = Ft$. The thermal equilibrium state cannot be attained owing to the boundary conditions, but a nonequilibrium stationary state satisfying $\partial P/\partial t = 0$ is realized after a transient time. Since we cannot get the nonequilibrium stationary state analytically, we show the numerical results of the Langevin equation Eq. (16).

Figure 10(a) shows the average frequency profiles $\omega_j$ for $L_y = 50$, 100, and 150 at $T = 1$, $K = 2$, and $F = 0.2$. The frequency profiles overlap with each other near the boundaries. The average frequency becomes almost zero near the center $j \simeq L_y/2$. Figure 10(b) shows the average value of $\sin(\phi_{j+1} - \phi_j)$ for $L_y = 50$, 100, and 150 at the same parameter values, since there are no vortices in one-dimensional
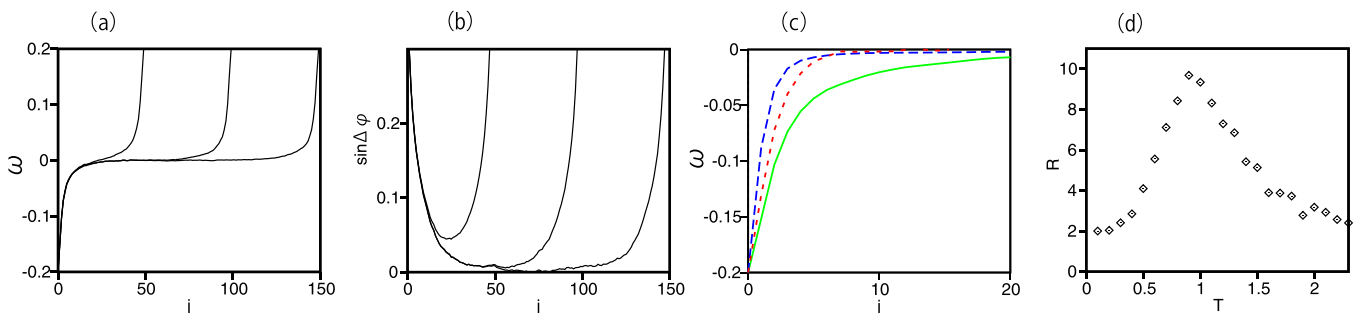


FIG. 10. (a) Average frequency profile $\omega_j$ at $L_y = 50$, 100, and 150 at $T = 1$, $K = 2$, and $F = 0.2$. (b) Average value of $\sin(\phi_{j+1} - \phi_j)$ for $L_y = 50$, 100, and 150. (c) Average frequency profiles at $T = 0.5$ (dotted red curve), 1 (solid green curve), and 1.5 (dashed blue curve) for $L_y = 100$. (d) Relationship between the temperature $T$ and the length scale $R$ of the boundary layers.

systems. The average value $\langle\sin(\phi_{j+1}-\phi_j)\rangle$ satisfies

$$\langle\sin(\phi_{j+1}-\phi_j)\rangle = \langle\sin(\phi_j-\phi_{j-1})\rangle + \omega_j/K. \qquad (19)$$

Near the center $j \simeq L_y/2$, $\langle\sin(\phi_{j+1}-\phi_j)\rangle$ and $\omega_j$ are almost zero. That is, an almost equilibrium state is attained in the central region. The nonequilibrium state is realized only near the boundaries. Figure 10(c) shows the frequency profile at $T = 0.5$ (dotted red curve), 1 (solid green curve), and 1.5 (dashed blue curve) for $L_y = 100$. The spatial scale of the nonequilibrium boundary layer is the largest at the intermediate value $T = 1$. The spatial scale of the nonequilibrium state can be evaluated at

$$R = \frac{2\sum_{j=1}^{L_y/2}|\omega_j|}{F} \qquad (20)$$

from the approximation of the integral of $|\omega|$ from $j = 1$ to $j = L_y/2$ by the triangular area $RF/2$. Figure 10(d) shows the relationship between $T$ and $R$. $R$ takes a peak value near $T = 0.9$. Interestingly, the spatial scale of the boundary layer takes the maximum at a finite temperature.

## V. SUMMARY

We have studied a vortex motion in coupled noisy phase oscillator lattice under shear stress. We have shown that the vortex motion can be approximated as a random walk in a tilted potential. When the temperature is high, many vortices are spontaneously generated. Owing to the glide motion of vortices, desynchronization is induced, and a nonzero frequency profile appears. When the vortex density is relatively small, the frequency profile is a linear function of $j$, which corresponds to the linear shear flow in the Newtonian fluid.

When the vortex density increases, the vortex density becomes nonuniform, or the vortex density increases near the boundaries where the shear stress is applied. The frequency profile is rather flat in the central region, and the slope of the frequency increases with the distance from $j = (L_y + 1)/2$. The nonlinear frequency profiles are related to the increase of the vortex density near the boundaries. A similar nonlinear response of the average frequency was observed even if the boundary conditions were changed to the conditions that the phase velocities are fixed to $\pm\omega_0$ at the top and bottom boundaries. The nonlinear response might be interpreted as the boundary layer effect, as shown in Fig. 7 for larger systems. The boundary layer effect was observed even in one- and three-dimensional systems. Our numerical results suggest that the nonequilibrium state is localized near the boundaries, and an almost equilibrium state is realized in a bulk region except for the boundary layers.

Our model is a simple model of coupled noisy oscillators with nonzero natural frequencies $f_{i,j}$ only at the boundaries $j = 1$ and $L_y$. The boundary oscillators play the role of pacemakers. Our model can also be interpreted as a nonequilibrium $XY$ model and a simple model of plastic motion in solids. The nonlinear velocity profile is often observed in plastic flows. Our simple model might help us qualitatively understand the complex behavior of plastic flows.

In this paper, we have studied the simplest case of coupled noisy phase oscillator lattices; however, we would like to study more general cases such as coupled noisy oscillators with the inertia term in the future. We have shown only numerical results in this paper, and the theoretical understanding is left to future study.

[1] Y. Kuramoto, in *International Symposium on Mathematical Problems in Theoretical Physics*, edited by H. Araki, Lecture Notes in Physics (Springer, Berlin, 1975), Vol. 39, p. 420.

[2] Y. Kuramoto, *Chemical Oscillations, Waves, and Turbulence* (Springer, New York, 1984).

[3] H. Sakaguchi and Y. Kuramoto, Prog. Theor. Phys. **76**, 576 (1986).

[4] S. Strogatz, Physica D **143**, 1 (2000).

[5] E. Ott and T. M. Antonsen, Chaos **18**, 037115 (2008).

[6] H. Sakaguchi, S. Shinomoto, and Y. Kuramoto, Prog. Theor. Phys. **77**, 1005 (1987).

[7] H. Hong, H. Chate, H. Park, and L. H. Tang, Phys. Rev. Lett. **99**, 184101 (2007).

[8] W. T. Read, *Dislocations in Crystals* (McGraw–Hill, New York, 1953).

[9] A. H. Cottrell, *Dislocations and Plastic Flow in Crystals* (Clarendon Press, London, 1953).

[10] J. J. Gilman, J. Appl. Phys. **36**, 3195 (1965).

[11] M. L. Falk and J. S. Langer, Phys. Rev. E **57**, 7192 (1998).

[12] A. Onuki, J. Phys.: Condens. Matter **15**, S891 (2003).

[13] H. Sakaguchi, Phys. Rev. E **105**, 054211 (2022).

[14] J. M. Kosterlitz and D. J. Thouless, J. Phys. C: Solid State Phys. **6**, 1181 (1973).

[15] A. P. L. Turner Jr. and T. Vreeland Jr., Acta Metall. **18**, 1225 (1970).

[16] P. Reimann, C. Van den Broeck, H. Linke, P. Hänggi, J. M. Rubi, and A. Pérez-Madrid, Phys. Rev. Lett. **87**, 010602 (2001); H. Sakaguchi, J. Phys. Soc. Jpn. **75**, 124006 (2006).

[17] E. Heinsalu, M. Patriarca, and F. Marchesoni, Phys. Rev. E **77**, 021129 (2008); M. Evstigneev, S. von Gehlen, and P. Reimann, *ibid.* **79**, 011116 (2009).

[18] Y. Pomeau, S. Zaleski, and P. Manneville, Phys. Rev. A **27**, 2710 (1983).

[19] K. Kawasaki, Prog. Theor. Phys. Suppl. **79**, 161 (1984).

[20] L. D. Landau and E. M. Lifschitz, *Fluid Mechanics* (Pergamon, London, 1959).

[21] G. Zocchi, E. Moses, and A. Libchaber, Physica A **166**, 387 (1990).

[22] E. C. Bingham, *Fluidity and Plasticity* (McGraw–Hill, New York, 1922).

[23] J.-B. Salmon, A. Colin, S. Manneville, and F. Molino, Phys. Rev. Lett. **90**, 228303 (2003),

[24] I. Kunita, K. Sato, Y. Tanaka, Y. Takikawa, H. Orihara, and T. Nakagaki, Phys. Rev. Lett. **109**, 248303 (2012).